Published in final edited form as:
Dev Biol. 2011 May 15; 353(2): 331–343. doi:10.1016/j.ydbio.2011.03.008.

Nav2 hypomorphic mutant mice are ataxic and exhibit abnormalities in cerebellar development

Elizabeth M. McNeill[*,†], **Mariana Klöckner-Bormann**[†], **Elizabeth C. Roesler**[†], **Lynn E. Talton**[‡], **Dieder Moechars**[§], and **Margaret Clagett-Dame**[*,†,‖,¶]

[*] Interdepartmental Graduate Program in Nutritional Sciences, University of Wisconsin, Madison, WI

[†] Department of Biochemistry, University of Wisconsin, Madison, WI

[‡] Behavioral Testing Core Facility, University of California, Los Angeles, CA

[§] Johnson & Johnson Pharmaceutical Research and Development, Beerse, Belgium

[‖] Pharmaceutical Science Division, University of Wisconsin, Madison, WI

Abstract

Development of the cerebellum involves a coordinated program of neuronal process outgrowth and migration resulting in a foliated structure that plays a key role in motor function. Neuron navigator 2 (*Nav2*) is a cytoskeletal-interacting protein that functions in neurite outgrowth and axonal elongation. Herein we show that hypomorphic mutant mice lacking the full-length *Nav2* transcript exhibit ataxia and defects in cerebellar development. At embryonic day (E)17.5, the mutant cerebellum is reduced in size and exhibits defects in vermal foliation. Reduction in cell proliferation at early times (E12.5 and E14.5) may contribute to this size reduction. The full-length *Nav2* transcript is expressed in the premigratory zone of the external granule layer (EGL). Granule cells in the germinal zone of the EGL appear to proliferate normally, however, due to the reduction in cerebellar circumference there are fewer total BrdU-labeled granule cells in the mutants, and these fail to migrate normally toward the interior of the cerebellum. In *Nav2* hypomorphs, fewer granule cells migrate out of cerebellar EGL explants and neurite outgrowth from both explants and isolated external granule cell cultures is reduced. This suggests the formation of parallel axon fibers and neuronal migration is disrupted in *Nav2* mutants. This work supports an essential role for full-length *Nav2* in cerebellar development, including axonal elongation and migration of the EGL neurons.

INTRODUCTION

Neuron navigator 2 (*Nav2*) was first identified as an all-*trans* retinoic acid (atRA)-responsive gene in the human neuroblastoma SH-SY5Y cell line (Merrill et al, 2002, 2004). It is a member of the neuron navigator family that also includes *Nav1* and *Nav3* (Maes et al., 2002). NAV2 is the closest in protein sequence of the navigator family members to the homolog *C. elegans* UNC- 53, which plays an essential role in longitudinal migration of

[¶]Corresponding author: Margaret Clagett-Dame, Ph.D., Department of Biochemistry, University of Wisconsin-Madison, 433 Babcock Drive, Madison, WI 53706-1544 USA, Phone: 608-262-3450, FAX: 608-262-7122, dame@biochem.wisc.edu.

several cell types including neurons, developing sex myoblasts and the excretory cell (Stringham et al., 2002). *unc-53* is required for normal mechanosensory neuron elongation (Hekimi and Kershaw, 1993). The importance of *Nav2* in axonal elongation was forged by two pieces of experimental evidence. RNA interference studies in SH-SY5Y cells showed that *Nav2* is necessary for atRA-mediated neurite outgrowth, and in *C. elegans unc-53* mutants, human *Nav2* could largely rescue the mechanosensory elongation defect (Clagett-Dame et al., 2006; Muley et al., 2008). Thus, *Nav2* is an ortholog to *unc-53* in the support of axonal elongation.

In cells, NAV2 associates with cytoskeletal elements, and a cytoskeletal interacting domain conferring this activity has been identified by truncation analysis (Muley et al., 2008). Neuron navigator family members are reported to co-localize with the plus-ends of microtubules in HeLa cells (van Haren et al., 2009). *unc-53* has also been suggested to play a role in cytoskeletal rearrangement through an interaction with *abi-1* as a part of the WAVE complex to regulate the *arp2/3* complex (Schmidt et al., 2009).

A *Nav2* (*unc-53H2*) hypomorphic mutant mouse lacking the full-length transcript primarily expressed in the nervous system, but containing a splice variant that starts upstream of exon 13, shows impaired acuity of several sensory systems in behavioral tests (Peeters et al., 2004). Our group has recently shown that *Nav2* is required *in vivo* for the normal development of cranial nerves IX (glossopharyngeal) and X (vagus), and in the adult mutant, the baroreceptor response requiring the function of these nerves is defective (McNeill et al., 2010).

Although *Nav2* is very highly expressed in the developing brain (Merrill et al., 2002; Peeters et al., 2004) very little is known about how it functions in the developing CNS. In this report, cerebellar development is studied in the *Nav2*/*unc-53H2* hypomorphic mutant mouse. Using a combination of behavioral tests, along with morphological analysis and gene expression studies, an essential role for *Nav2* in granule cell development and foliation of this brain region is revealed.

METHODS

Animal generation

All animal studies were performed under an approved ACUC animal protocol according to institutional guidelines at the University of Wisconsin, Madison. *Nav2* (*unc-53H2*) mice were obtained (Peeters et al., 2004) and backcrossed onto a C57/Bl6Hsd background for 4 or more additional generations. Studies were conducted using $Nav2^{+/-} \times Nav2^{+/-}$ and female $Nav2^{+/-}$ × male $Nav2^{-/-}$ crosses. Embryos or pups were collected at the indicated embryonic or postnatal stages. Noon the day of vaginal plug detection was considered E0.5. Genotyping was performed on tail samples using the Direct PCR Lysis Reagent (Viagen Biotech, Los Angeles, CA) and primer sets described previously (Peeters et al., 2004).

Behavioral tests

Gait test—Mice (8 male homozygote and 10 male wild-type) at approximately 5 months of age were given three habituation trials after which all subjects completed the run rapidly and entered the escape box readily, followed by the test trial. The following measures were analyzed: distance from center (deviation from the center of the runway; distance from center is calculated by finding the midpoint of a line drawn from the midpoint of each left-hind limb step to the closest midpoint of a right-hind limb step); number of steps taken; side width (lateral distance between the paths of the forelimb and hind limb on the same side), and the distance from one edge (calculated by finding the midpoint of the line drawn from

the midpoint of each left hind limb step to the closest midpoint of a right hind limb step followed by determination of the perpendicular distance of that point to the left side).

Balance beam test—Mice were placed in the center of the beam (1.9 cm diameter × 122 cm length) for a 3 min habituation trial on day one. On day two, escape boxes (8 cm × 8 cm × 18 cm) were added to both ends of the beam. The mice were placed on the center of the beam for three trials of up to 3 min each with a 1 min interval. During habituation and testing trials, latency to enter the escape boxes, number of falls, number of beam segments crossed (5 cm), number of 180° turns, number of grooming bouts, and hanging from the beam were measured.

Rotorod test—Mice were placed onto a cylinder that rotated at either a constant or accelerating speed. The cylinder was divided into 5 compartments with an infra-red sensor that automatically recorded an animal's fall. The latency to fall from the cylinder and cylinder rotation speed were also recorded. In the acceleration test, rod speed increased from an initial speed of 5 rpm to a maximum of 60 rpm over a period of 300 s.

Stereotyped behavior—Mice were individually placed in a large Plexiglass cylinder (30 cm diameter × 45 cm height) standing on an elevated metal grid and they were then videotaped in a quiet room under dim lighting conditions for a period of 10 min. Videotapes were later scored by a blinded observer (every 2 s; 300 samples/mouse) for a variety of behaviors including walking, grooming, leaning, counter-clockwise turning, clockwise turning, climbing, rearing and standing still. Student's T-test was used for statistical analysis of all behavioral tests.

Tissue collection and fixation

Animals (P0 and older) were anesthetized and perfused transcardially with cold phosphate buffered saline (PBS, pH 7.4), followed by perfusion with cold 4% paraformaldehyde (PFA) in phosphate buffer (0.1 M, pH 7.4). The brain was dissected from the skull and fixed at 4°C 24–72 h in 4% PFA. For embryos, the head (E17.5) or entire embryo (E12.5 and E14.5) were fixed directly in 4% PFA. Tissues were washed in PBS and dehydrated though a graded methanol series in PBS, followed by equilibration in 100% methanol and storage at 4°C until use.

Brains at E17.5 and P0 used for Ki67 immunohistochemistry were processed using Dent's fixative (4 MeOH:1 DMSO). Heads were placed in fixative for 24 h at 4°C and then dissected in methanol. Dent's fixed brains were washed thee times in 100% methanol and stored as above.

Cerebellar explant and dissociated granule cell culture

Cerebellar microexplant cultures were set up as described (Nakatsuji and Nagata, 1989; Engelkamp et al., 1999). Cerebella were dissected at P0, and strips of EGL were removed, cut into small pieces, and cultured in laminin (0.1mg/ml) coated Nunc Labtek II chamber slides for 72 h. Cultures were fixed in cold 1:1 methanol:acetone followed by staining with antibodies to NCAM and Pax6. Images were taken using a TE2000 microscope.

Dissociated cerebellar external granule cells were cultured as described by Trenkner and Sidman, 1977; Hatten, 1985; and Tahirovic et al., 2010 with minor modifications. Briefly, strips of the EGL were dissected from the cerebella at P0/P1 and placed in 1 ml of solution containing trypsin (0.05%; Invitrogen, Carlsbad, CA) and DNAse (10,000 U; Roche Applied Science, Indianapolis, IN) and dissociated by trituration. Dissociated cells were cultured on poly-D-lysine (Sigma, St. Louis, MO) coated coverslips in 12-well plates at a density of 2

$\times 10^5$ cells per well in neurobasal-serum free medium containing the following percentages of stock solutions: 2% of a 50x B27 supplement, 1% L-glutamine (200 mM) and 1% penicillin/streptomycin (10,000 U and 10,000 μg, respectively per ml) (Invitrogen, Carlsbad, CA). Cells were incubated for 48 h at 37 °C in 5% CO_2.

Vibratome *in situ* hybridization

A partial *Nav2* rat probe (474 bp) 93% identical to mouse (Merrill et al., 2002), and specific to the long *Nav2* transcript was used for *in situ* hybridization carried out in sagittal vibratome slices (200 μm) as previously described (Wilkinson, 1998; Kaiser et al., 2003; See et al, 2009). A probe to the 3′ end of the *Nav2* transcript designed to detect both the full-length *Nav2* transcript as well as the shorter splice variant was amplified from P21 mouse cerebellum using the following upstream 5′ GAAAGAGCCAGGCAGCGCCA 3′ and downstream 5′ TCCCAGCCCTCGGTCACTCG 3′ primers amplifying a 644 bp piece. The following probes were also produced using the primers listed. *Reelin:* 5′ GCTCGTGGTTTCCGGGGTGG 3′ and 5′ ATGCCCGCTGCAGAGCTTGG 3′ 625 bp, *Math1*: 5′ CAACGACAAGAAGCTGTCCA 3′ and 5′ ACAACCATCACCACAGACCA 3′ 609 bp, *Pax6*: 5′AGGGGGAGAGAACACCAACT 3′ and 5′ ATAACTCCGCCCATTCACTG 3′ 562 bp. Vibratome sections were photographed using a Nikon model SMZ-U dissection microscope fitted with a 1X lens, Qimaging camera and MetaMorph V6.3 software (Molecular Devices, Downington, PA).

Quantitative PCR

Total RNA was isolated from the whole cerebellum (n=3 wild-type and 3 mutants) at P0 and P7 using Trizol according to the manufacturer's recommendations (Invitrogen, Carlsbad, CA). The RNA was treated with DNase, and purified using a RNeasy column according to the manufacturer's recommendations (Qiagen, Valencia, CA). Total RNA (1 μg) was reverse transcribed using MultiScribe reverse transcriptase and random primers (High Capacity cDNA Reverse Transcription kit, Applied Biosystems, Carlsbad, CA), diluted 1:200, and used in subsequent PCR analysis. The quantitative polymerase chain reaction (Q-PCR) assay was performed using the real-time LightCycler system (Roche, Indianapolis, USA) with LightCycler Faststart DNA Master SYBR Green 1 kit (Roche) according to the manufacturer's protocols. Expression was normalized using hypoxanthine guanine phosphoribosyl transferase 1 (*HPRT*) levels for each sample.

Histology and Immunohistochemistry

Brains were embedded in paraffin and sectioned at 4 or 10 μm. Additional adult brains were sectioned at 30 μm by Neuroscience Associates (Knoxville, TN). Nissl (cresyl violet) staining was performed as described (Bancroft and Stevens,1990). Immunohistochemistry was performed on sections (10 μm) containing the vermal region of the cerebellum in sagittal orientation as well as in cerebellar explants and dissociated granule cell cultures. The following primary antibodies were used: calbindin d28k (Clone CB-955, Sigma, St. Louis, MO, mouse IgG, 1:1000), Abi-1 (Abnova, Taiwan, rabbit IgG, 5 μg/ml), NCAM (L1, Millipore, Billerica, MA, rat IgG, 4 μg/ml), alpha tubulin, (Clone B-5-1-2, Sigma, St. Louis, MO, mouse IgG, 2 μg/ml), Pax6 (Covance, Princeton, NJ, rabbit IgG, 7 μg/ml) and Ki-67 (Clone B56, BD Pharmingen, SanJose, CA, mouse IgG, 1 μg/ml 1:250). Alpha tubulin was incubated with anti-mouse alexa 594 (Invitrogen, Carlsbad, CA, 2 μg/ml) and then counter stained with DAPI (Invitrogen, Carlsbad, CA). Pax6 and NCAM L1 were incubated with anti-rabbit alexa 488 and anti-rat alexa 594 (2 μg/ml), respectively. Abi-1 was incubated with anti-rabbit alexa 594 (2 μg/ml). Calbindin d28k and Ki-67 slides were incubated with Vectastain® Peroxidase Mouse IgG followed by incubation with Vectastain® ABC Reagent, color development using Sigma FAST® DAB and Buffer H_2O_2 tablets. All slides for each colorimetric antibody experiment were developed for the same amount of time. A

subset of slides was counter-stained using Nissl stain, followed by imaging using a Nikon TE2000 microscope. The groups (n=individual animals) were compared by Student's T-test.

BrdU and Apoptosis Analyses

Intraperitoneal injections of a 10 mg/ml solution of bromodeoxyuridine (BrdU) in PBS were administered to pregnant females (50 μg/g) at E12.5, E14.5 and E17.5 or to pups at P0 pups (10 μg/g). Animals were euthanized 2 h later in order to assess cell proliferation. To evaluate granule cell migration, pregnant females were injected 40–48 h before birth, and pups were evaluated at P0. Tissue was collected, fixed, and embedded in paraffin. Sections (4 μm) placed on ultrastick slides (Ted Pella Inc., Redding, CA) were subjected to trypsin digestion. The primary BrdU antibody was diluted to a final concentration of 6 μg/ml (Clone BU-20a, DakoCytomation, Denmark). Tissue was then incubated with biotinylated anti-mouse IgG and the Vectastain ABC avidin-biotinylated HRP reagent (Vector Laboratories, Burlingame, CA). Following antibody staining, substrate was added as described above. BrdU-positive cells were counted and the circumference and/or area of the cerebellum was assessed using MetaMorph v6.3 analysis software.

In situ cell death detection assay (TUNEL assay) was performed as described in the manufacturer's directions (Roche Applied Science, Indianapolis, IN) on 4% PFA fixed 4 μm sections from 3 wild-type and 3 mutant embryos both at E 12.5 and E14.5. False positives were eliminated by evaluation of sections at both 488 and 594 nm (autofluorescence). A positive control (DNase-treated sections) was included in all assays.

Analysis of cell migration and neurite outgrowth

Cerebellar explant cultures were scored for cell migration and for neurite outgrowth. Explants in which no or few cells migrated away from the tissue received a score of "0", and those in which either a moderate or large number of cells had migrated received a "1" or "2", respectively. In similar fashion, extension of no or few neurites was given a "0", whereas moderate or extensive neurite outgrowth was scored as a "1" or "2", respectively. The scores for each animal were averaged, and individual animal values were used for comparison of the wild-type and hypomorphic mutant groups by Student's T-test.

Dissociated granule cell cultures were stained with antibodies to Pax6 and alpha tubulin as well as Dapi and were imaged (minimum of 25 random fields at 400x); only cells that stained positive for both Pax6 and alpha tubulin were counted (approximately 60 cells/animal were evaluated). The width of the cell body, and the length of processes extending from the cell body were measured individually in pixels using the region measurements tool in the Metamorph imaging system. The number of neurons with processes longer than one cell body in diameter was determined.

RESULTS

Nav2 hypomorphic mutant mice exhibit deficits in motor coordination and balance

During the course of working with the *Nav2* homozygous mutants, we noted that these mice exhibited ataxia, with the effect becoming obvious in most mutants by about 4 weeks of age (Movie 1). To examine the behavior of these mice more closely, a number of studies were performed, including gait, balance beam, rotorod and stereotyped behavior tests.

In gait analysis, *Nav2* hypomorphic mutants demonstrated a significant deviation from normal in many measures. Mutants were found significantly further from the center of the runway than wild-type mice (Figure 1A), showed an increase in the average number of steps taken (Figure 1B) and had an average side width that was larger on the left side (Figure 1C).

The distance to the center of the hind limb paths, as measured perpendicular to the left edge, was larger in homozygote hypomorphic mutant mice, and homozygotes showed a significant preference for the right side of the runway (data not shown).

Balance beam activity studies showed that the *Nav2* hypomorphic mutants traveled a greater distance on the beam and had an increased number of missteps when compared to the wild-type controls (Figure 1D and E).

In the constant speed rotorod test, *Nav2* mutants showed a decreased average latency to drop from the apparatus (11 s) as compared to wild-type animals (140 s, Figure 1F). In the accelerating rotorod tests, the mutant animal latency to fall was ~22 s, or about half of the latency to fall for wild-types (44 s, Figure 1G). The speed at which the homozygotes fell off the rotorod (23 rpm) was also significantly lower than in the wild-type animals (44 rpm, Figure H).

In 10 min sessions of stereotyped behavior, *Nav2* hypomorphic mutants spent a decreased percentage of time exhibiting rearing behavior (Figure 1I). Hypomorphs also exhibited a significant increase in the percentage of time spent rotating with no directional preference (Figure 1J). Finally the hypomorphs spent significantly more time overall in active behaviors, i.e. grooming or walking, indicating hyperactivity (Figure 1K). Taken together, the deficits in performance in several behavioral tests showed the motor coordination and balance of *Nav2* hypomorphic mutants to be impaired.

The morphology of the cerebellum is abnormal in adult *Nav2* hypomorphic mutants

Because the behavioral phenotypes observed in *Nav2* homozygous mutant animals were highly similar to those reported in animals with cerebellar ataxia (Lalonde and Strazielle, 2007), the morphology of the cerebellum was examined more closely. Macroscopic examination of the cerebellum of adult wild-type mice showed the normal external lobule morphology (5/5; Figure 2A). The medial foliation along the anterior posterior (AP) axis of the central region (vermis) was well delineated and distinct from that of the lateral extensions (hemispheres). In contrast, 100% of hypomorphic mutant mice showed abnormal folding in the vermal region of the cerebellum (11/11; Figure 2B). By external analysis, the vermis appeared abnormal on the right side of 9 of the 11 homozygote mutants examined and on the left side in the remaining 2 homozygotes. A medial section (10 μm) from the wild-type brain showed the expected lobules (I/II–X), including a VI–VII lobe containing a well-developed intercural fissure (Figure 2C, closed arrowhead). In *Nav2*$^{-/-}$ mutants, the VI–VII lobe was severely hypoplastic and no intercural fissure was observed (Figure 2D, open arrowhead). In addition, whereas the wild-type brain contained three distinct folia encompassing I–V (I/II, III, and IV/V), only two were apparent in the homozygote. Analysis of 10 μm serial sections through the entire vermis of the homozygote brain revealed that abnormal foliation was seen on both the right and left side of the brain region (Figure S1).

In order to evaluate the prevalence and severity of the abnormalities seen in the mutant, medial sections (10 or 30 μm) from 6 wild-type and 12 *Nav2*$^{-/-}$ mutants were examined. All the wild-type brains showed the expected pattern of foliation, whereas all homozygotes showed hypoplasia of folia VI–VII and absence of the intercural fissue (Figure 2G). The majority (8/12) of the hypomorphic mutants also showed only two apparent folia in the regions of I–V. Despite the abnormalities in foliation, the overall cytoarchitecture (molecular layer, Purkinje cells, and inner granule cell layer) in the folia of homozygous mutant mice appeared grossly similar to that of the wild-type controls (Figure 2E, F).

Nav2 mRNA is expressed in the developing cerebellum

Nav2 expression in the developing cerebellum was examined in vibratome sections of wild-type and hypomorphic mutant mice using an *in situ* probe anchored in the 5′ region of the full length *Nav2* transcript, and another directed to the 3′ region that should detect all known transcripts. Sagittal sections taken from a wild-type cerebellum and hybridized to the 5′ probe revealed *Nav2* expression in the EGL at E17.5, P0 and P7 (Figure 3A–C,D,I). The EGL is a transient cell layer comprised of two specific zones, a superficial outer layer of proliferating cells also called the germinal layer or zone (gz), and a deeper zone containing premigratory postmitotic granule cells called the premigratory layer (pml) (Cajal, 1911). Specific expression of the full-length transcript (blue-purple in Figure 3D, I) was observed in the deeper premigratory layer of the EGL bordering the Purkinje cell plate or layer (pcp and pcl, respectively) that was not stained, but appeared naturally brown in coloration. Low-levels of full-length *Nav2* were also observed in the IGL (inner granule layer) at P14 and P21 (data not shown). As expected, no specific staining with the 5′ probe was observed in the *Nav2*$^{-/-}$ mutant (Figure 3F and 3K), nor was specific staining seen when the control 5′ sense probe was used (data not shown). The 3′ probe (detects both the long and short transcript), showed the expected staining of the inner layer (pml) of the EGL at P0 and P7 (Figure 3E and 3J), and no staining was observed with the sense control probe (Figure 3H and 3M). In the hypomorphic mutant mouse, specific staining with the 3′ probe was not observed (compare Figure 3E to 3G and 3J to 3L), indicating that loss of the full-length transcript does not cause a compensatory increase in the smaller *Nav2* transcript, and that in the normal mouse, the long transcript predominates in the EGL. Therefore, at least in the EGL, the hypomorphic mutant appears to represent a true null for *Nav2* expression.

Analysis of cerebellar foliation and size through development

Because cerebellar fissure formation begins in the embryo (~E17) and continues into postnatal life, histological analysis of midsagittal sections through a time course of development was performed. This analysis revealed abnormalities in foliation in addition to a reduction in the size of the cerebellum as early as E17.5 in *Nav2* hypomorphic mutant mice (Figure 4). Wild-type brains at E17.5 showed the initiation of four fissures: preculminate (pc), primary (pr), secondary (sec), and posterolateral (pl). In the mutant, a delay in fissure formation was seen in these regions at E17.5 and P0 (Figure 4B and 4D). In all hypomorphic mutant animals examined, there was an overall decrease in the size of the central lobe from which lobes VI–VIII arise (Sillitoe and Joyner, 2007). By P7, the foliation pattern of the mutant was clearly abnormal, and this became even more obvious by P17 (Figure 4F and 4H).

The size of the cerebellum decreased with development in the hypomorphic mutant mice compared to their wild-type counterparts (Figure 5A). To further address whether a reduction in cell proliferation or an increase in apoptosis might account for the reduction in the size of the cerebellum in mutant embryos, BrdU incorporation and TUNEL staining were performed at E12.5 and E14.5. There was a small but non-statistically significant reduction in BrdU incorporation in the cerebellar primordium at both of these time points, whereas the number of labeled cells in the rhombic lip appeared unchanged (Figure 5B and 5C). There were very few cells undergoing apoptosis in either the wild-type or mutant cerebella (data not shown). Thus, the small reduction in proliferating cells in the cerebellar primordium at E12.5 and 14.5 could be biologically important, and may have contributed to the decreased size of this brain region at later times.

Purkinje cell development

Purkinje cells were examined after antibody staining for calbindin d28k, a specific marker for the perikaryonic region and dendrites. No differences were observed between wild-type

and homozygote mutants in the development of the Purkinje cell plate at P0, and Purkinje cell development between P7 and P15 appeared grossly undisturbed in *Nav2*$^{-/-}$ hypomorphs (Figure 6 and data not shown). Although the circumference of the mutant cerebellum at P7 was significantly reduced compared to that of the wild-type cerebellum, the total number of Purkinje cells through vermal sections was very similar, resulting in tighter packing of the Purkinje cells (Figure 6D). This tighter packing persisted in the adult hypomorphic mutant (Figure 2 compare E to F). At P7, when the initiation of the intercural fissure that separates lobes VIb and VII should be taking place, a focal abnormality was noted in the distribution of both the Purkinje and granule cells in this region in the homozygote mutant (compare Figure 6B to 6A). At P8 missing or misplaced Purkinje cells and a thinning of the EGL were also noted in the region of the *Nav2* mutant where folia VII should be forming, suggesting that in the mutant, this lobe is largely underdeveloped or missing (Figure 6C).

Disappearance of the EGL is delayed in the *Nav2* hypomorphic mutant

Granule cells in the germinal zone of the EGL continue to proliferate for the first two postnatal weeks. Just prior to birth, granule progenitor cells begin to exit the cell cycle forming the postmitotic premigratory zone, and it is these cells that mature and migrate to form the IGL. This process is normally complete by P20, a few days after the disappearance of the EGL (Goldowitz and Hamre, 1998; Sillitoe and Joyner, 2007). At P15, the EGL appeared thicker in the *Nav2* hypomorphic mutant, and persisted through P17, a time when these cells in the wild-type littermate controls had already fully migrated to the IGL (Figure 7A).

To assess whether the increased thickness of the mutant EGL was due to an increased rate of progenitor cell proliferation, *in vivo* labeling was performed with BrdU. BrdU was administered at E17.5, P0, and P7; and the embryos or pups were taken 2 h later. At all times, a similar number of BrdU-labeled cells were present in the homozygote mutant and wild-type embryos in a 0.5 mm long region of the EGL (Figure 7B and data not shown) suggesting that the rate of granule cell proliferation was unchanged in the cells within a given lineal unit. However, it is important to note that the circumference of the homozygote mutant cerebellum at E17.5 was 72% of wild-type, and this size discrepancy increased with development, with homozygote mutant cerebella having a circumference of 48% that of wild-type at P0. Therefore, although within a defined segment of EGL the number of BrdU-labeled cells was similar, overall there were more BrdU labeled cells in the wild-type animals. Immunostaining with an antibody to Ki67 confirmed that the number of mitotically-active cells in a defined segment of tissue appeared similar at E17.5, P0 and P7 in the wild-type and mutant animals (Figure S2 and data not shown). These results indicate that persistence of the EGL in homozygotes is not due to increased proliferation of progenitor granule cells.

Nav2 is important in granule cell migration and parallel axon fiber formation

An alternative explanation for the persistence of the EGL in mutants could be a defect that prevents the normal differentiation and migration of this cell layer. To evaluate migration of the granule cells from the EGL, proliferating granule cells were labeled *in vivo* with BrdU, and the cerebellum was collected and analyzed approximately 2 days after the initial injection. As expected, in wild-type littermates, granule cells that had undergone proliferation at the time of BrdU injection had begun to differentiate and migrate away from the EGL toward the IGL in the cerebellum (Figure 7C). In contrast, in the *Nav2* hypomorphic mutant significantly more BrdU-labeled cells were present at P0 in the outermost cell layers (germinal zone) on the surface of the EGL, indicating these cells had not started to migrate toward the IGL as observed in wild-type littermate controls. This

result strongly suggests there is a defect in granule cell differentiation and/or migration that is responsible for persistence of the EGL in *Nav2* mutants.

The expression of genes known to be important in granule cell differentiation and migration was examined next at P0 and P7. *Math1* is required early for granule cell differentiation, and tight regulation of expression level continues to be important for differentiation of cerebellar granule cells in the EGL (Gazit et al., 2004; Helms et al., 2001). *Pax6* expression in granule cells is required for their differentiation and emigration from the EGL, processes that initiate close to the time of birth (Engelkamp et al., 1999), and *Reelin* is required for neuronal migration and positioning (Hevner, 2008). By *in situ* hybridization, *Math1, Pax6 and Reelin* mRNAs appeared unchanged in the EGL at P0 (Figure 8A–F). However, by P7, a change in the distribution of both *Math1* and *Pax6* mRNAs was observed, with a mixing of the layers of positive cells such that the expected gradations in expression in the EGL (*Math1* and *Pax6* darker), ML (*Pax6* nearly absent) and IGL (lighter *Pax6*) was less evident in the cerebellum of the hypomorphic mutants compared to wild-type controls (Figure 8 compare H,J, L, and N to G,I,K, and M, respectively). *Reelin* expression also appeared less well organized in both the outer and inner granule layers of the hypomorphic mutant mouse at P7 (Figure 8, compare P to O and R to Q). The overall level of these mRNAs was unchanged in the cerebellum as assessed by quantitative PCR at both P0 and P7 (Supplementary Table 1). The disorganized appearance of *Math1, Pax6* and *Reelin* mRNA expression at P7 provides additional evidence that granule cell differentiation and/or migration is perturbed in *Nav2* mutants.

Cerebellar explant cultures were performed to further examine the ability of granule cells in mutant mice to migrate and extend neurites. Granule cell bodies were identified using an antibody to Pax6 and neuronal processes were labeled using an antibody to NCAM L1. After 72 h in culture, granule cells from wild-type explants had begun to migrate out and extend processes (Figure 9A and 9C). In contrast, fewer granule cells migrated away from the cerebellar explants in hypomorphic mutants, and these explants showed significantly less neurite outgrowth that the wild-type explants (Figure 9B, 9D and 9E). To study this process in more detail, granule cells were isolated from the EGL at P0/P1 and cultured. There was a significant reduction in neurite outgrowth of granule cells from *Nav2* mutants compared to the wild-type controls (Figure 9F–H). Thus, the extension of granule cell axons is defective in *Nav2* hypomorphic mutant mice.

DISCUSSION

The cytoskeleton is highly dynamic and undergoes continuous remodeling during neuronal cell migration and axon growth. A growing body of literature suggests that the neuron navigator family of proteins play a role in cytoskeletal rearrangement (Muley et al., 2008; Schmidt et al., 2009; van Harren et al., 2009). *Nav2* is necessary for axonal elongation (Muley et al., 2008), the development of normal cranial nerve fiber density and connections in developing embryos (McNeill et al., 2010). Herein, we show that attainment of normal cerebellar size, foliation of the vermal region, axonal outgrowth, and granule cell migration are all dependent upon *Nav2*.

Cerebellar development and Foliation

The cerebellum arises from dorsal rhombomere 1 with cells from the ventricular zone contributing precursors (Purkinje cells and other non-granule cell neurons) starting at E10.5–11.5. The rhombic lip contributes granule cell precursors that begin to migrate at E13.5 to the outer edge of the cerebellar primordium (Chizhikov et al., 2006). There are two main stages in the morphogenetic process of folding of the cerebellum: formation of the cardinal lobes, which occurs embryonically (~E17 in mouse), and formation of the lobules

and sub-lobules (folia), which occurs postnatally (P0–P14; Sillitoe and Joyner, 2007). *Nav2* hypomorphic mutants contain the same overall compliment of cell types in the cerebellum as do wild-types at the onset of foliation (E17.5), suggesting that there is no defect in the ability of the progenitor cells to populate the cerebellum, however, the size of the cerebellum in the mutant is smaller. *Nav2* is found early in development at the midbrain-hindbrain border (Merrill et al., 2002: McNeill et al., 2010), suggesting that it could influence the development of the cerebellar primordium. Few apoptotic cells are normally found at E13.5 and 14.5 in the mouse cerebellum (Ishimura et al., 2008) and we found no evidence for any increase in apoptosis in the *Nav2* mutants compared to their wild-type counterparts, either at E12.5 or 14.5. Rather, the size reduction in mutants may be the result of a slight reduction in the number of cells undergoing proliferation, thus limiting the expansion of the cerebellar primordium during development.

Homozygote mutants also exhibit foliation defects, both during formation of the cardinal lobes with specific reduction in the formation of the preculminate and primary fissures, and during the development of folia I–V and VI/VII. This indicates that *Nav2* is playing an important role early in the folding process, and continues to play a role in folia formation postnatally.

The morphological changes observed in the mutant are functionally important, as evidenced by defects in motor coordination and gait. Many other genetic mutants that have aberrant folia formation exhibit ataxic behavior similar to that observed in the *Nav2* hypomorphic mutant, including *RORα*, *Grid2*, and *nervous* (Lalonde and Strazielle, 2007) as well as *TR4* (Chen et al, 2005), *Reeler* (Katsuyama and Terashima, 2009), and *NBS1* (Frappart et al, 2005).

A key event in initiation of foliation is the acquisition of distinct cytoarchitecture in anchoring centers that will become the base of each fissure. The outgrowth of the folia then proceeds in a self-sustaining manner driven by granule cell migration (Sudarov and Joyner, 2007). In the *Nav2* mutant there is proper initiation of all fissures (Figures 3 and 4) and thus, we believe the abnormal foliation observed in the mutant is a result of abnormal granule cell migration rather than an abnormality in initiation of foliation and formation of the anchoring centers.

Neuronal Migration

The full-length *Nav2* transcript is strongly expressed in the inner layer of the EGL at E17.5 in line with a functional role in the premigratory granule cell of the EGL. Consistent with this hypothesis, *Nav2* expression continues in this region through the peak of proliferation (P8–10; Fujita et al., 1966), persisting until EGL migration is complete.

Closer examination of the *Nav2* hypomorphic mutant EGL shows that it is thicker than that seen in the wild-type at P15 and P16, and is still present at P17, a time when migration should be largely complete (Miale & Sidman, 1961; Sillitoe and Joyner, 2007). As shown by short-term BrdU labeling and staining with Ki67, the increase in EGL thickness is not due to an increase in cell proliferation. However, analysis of granule cells labeled with BrdU and allowed to develop for an additional 2 days shows that labeled cells in *Nav2* mutants remain largely associated with the EGL, whereas those in the wild-type have begun to migrate toward the IGL. Persistence of the EGL has also been noted in *Pax6* (Engelkamp et al., 1999) and *TR4* mutants (Chen en al., 2005), and the increase in EGL size in these mice is likewise not due to an increase in proliferation of this cell layer but rather to a disturbance in postmitotic granule cell migration.

Axonal outgrowth

When granule cell precursors begin to exit the cell cycle and differentiate, they extend horizontal parallel axon fibers and undergo tangential migration within the premigratory layer of the EGL. They then switch from tangential to radial (vertical to the pial surface) migration along the Bergmann glial fibers, leaving the EGL cells to enter the ML and ultimately forming the IGL (Sillitoe and Joyner, 2007; Chédotal, 2010). Consistent with the previously defined role for *Nav2* in axonal elongation (Clagett Dame et al., 2006; Muley et al, 2008), we find that *Nav2* is needed for maturing granule cells to extend parallel axon fibers, as evidenced by the reduced ability of cells from mutants to exend processes, both in cerebellar microexplants and dissociated EGL cell cultures (Figure 9). *Pax6* mutants also fail to extend parallel axon fibers resulting in foliation defects and ataxia similar to those seen in the *Nav2* mutant (Engelkamp et al, 1999; Yamasaki et al, 2001).

Unc-53, the *C. elegans*, homologue of *Nav2*, has been linked to the Arp2/3 complex through an interaction with ABI-1 (Schmidt et al., 2009). Importantly, *Abi-1* is found in cerebellar granule cells (Proepper et al., 2007) where it could be playing a role along with NAV2 in granule cell axonal outgrowth and/or migration. *Abi-1* is essential for the formation and activation of the WAVE complex, leading to enhanced actin nucleation and remodeling via the Arp2/3 complex (Innocenti et al., 2003, 2004; Bompard and Caron, 2004; Takenowa and Suetsugu, 2007). Arp2/3 is known to mediate the local reorganization of the actin cytoskeleton at the leading edge of migrating cells (Higgs and Pollard, 2000). Interestingly, *Rac1* has recently been shown in cerebellar granule cells to recruit the WAVE complex including WAVE, SRA-1, NAP-1 and ABI-1 to the plasma membrane to enable actin remodeling through the Arp2/3 pathway, events needed for axonal outgrowth (Tahirovic, et al., 2010).

Additionally, Nav2 is found in cells associated with the cytoskeleton including microtubules and neurofilament proteins (Muley et al., 2008), and neuron navigator family members have recently been proposed to serve as plus end tracking proteins (+TIPs) coupling ATPase activity to a microtubule binding potential (van Haren et al., 2009). +TIPs influence microtubule dynamics and link microtubules to other cellular structures such as actin, cortically-bound factors, and intracellular membanes (Akhmanova and Steinmetz, 2008). Finely tuned actin filament organization and microtubule dynamics are essential for neuronal migration and axon growth and guidance (Luo, 2000; da Silva and Dotti, 2002; Dent and Gertler, 2003, Kawauchi and Hoshino, 2008; Witte and Bradke, 2008). Future studies are needed to determine whether *Nav2* could serve as a link between actin remodeling and microtubule dynamics during neurite outgrowth.

Using the *Nav2*/*unc-53H2* hypomorphic mutant mouse, we have established that mammalian *Nav2* plays a key role in the attainment of normal cerebellar size, as well as in cerebellar granule cell differentiation and migration. Disturbance of postmitotic granule cell parallel axon fiber extension and subsequent perikaryal translocation of the nucleus may underlie the failure of these cells to migrate properly from the EGL, thus leading to defects in cerebellar foliation and ataxia in this mutant. *Nav2* has been shown to facilitate cytoskeletal rearrangement and neurite outgrowth in cell culture. The results presented here establish an *in vivo* role for *Nav2* in the development and proper formation of the cerebellum.

Supplementary Material

Refer to Web version on PubMed Central for supplementary material.

Acknowledgments

We thank Laura Vanderploeg and Robin Davies in the Biochemistry Media Lab for figure artwork and movie editing. E.M. McNeill was supported in part by a fellowship from NIH T32 DK07665 and a PEO Scholar award.

References

Akhmanova A, Steinmetz MO. Tracking the ends: a dynamic protein network controls the fate of microtubule tips. Nat Rev. 2008; 9:309–322.

Bancroft, JD.; Stevens, A. Theory and practice of histological techniques. 3. Churchill Livingstone; London: 1990.

Bompard G, Caron E. Regulation of WASP/WAVE proteins: making a long story short. J Cell Bio. 2004; 166:957–962. [PubMed: 15452139]

Cajal, SR. Texture of the nervous system of man and the vertebrates. Springer-Verlag/Wien; New York: 1911. 2000

Chédotal A. Should I stay or should I go? Becoming a granule cell. Trends Neurosci. 2010; 33:163–172. [PubMed: 20138673]

Chen YT, Collins LL, Uno H, Chang C. Deficits in motor coordination with aberrant cerebellar development in mice lacking testicular orphan nuclear receptor 4. Mol Cell Biol. 2005; 25:2722–32. [PubMed: 15767677]

Chizhikov VV, Lindgren AG, Currie DS, Rose MF, Monuki ES, Millen KJ. The roof plate regulates cerebellar cell-type specification and proliferation. Development. 2006; 133:2793–2804. [PubMed: 16790481]

Clagett-Dame M, McNeill EM, Muley PD. Role of all-*trans* retinoic acid in neurite outgrowth and axonal elongation. J Neurobiol. 2006; 66:739–56. [PubMed: 16688769]

DaSilva JS, Dotti CG. Breaking the neuronal sphere: regulation of the actin cytoskeleton in neuritogenesis. Nature. 2002; 3:694–704.

Dent EW, Gertler FB. Cytoskeletal dynamics and transport in growth cone motility and axon guidance. Neuron. 2003; 40:209–227. [PubMed: 14556705]

Engelkamp D, Rashbass P, Seawright A, van Heyningen V. Role of *Pax6* in development of the cerebellar system. Development. 1999; 126:3585–96. [PubMed: 10409504]

Frappart PO, Tong WM, Demuth I, Radovanovic I, Herceg Z, Aguzzi A, Digweed M, Wang ZQ. An essential function for NBS1 in the prevention of ataxia and cerebellar defects. Nat Med. 2005; 11:538–44. [PubMed: 15821748]

Fujita S, Shimada M, Nakamura T. H^3-thymidine autoradiographic studies on the cell proliferation and differentiation in the external and the internal granular layers of the mouse cerebellum. J Comp Neurol. 1966; 128:191–208. [PubMed: 5970298]

Gazit R, Krizhanovsky V, Ben-Arie N. Math1 controls cerebellar granule cell differentiation by regulating multiple components of the Notch signaling pathway. Development. 2004; 131:903–13. [PubMed: 14757642]

Goldowitz D, Hamre K. The cells and molecules that make a cerebellum. Trends Neurosci. 1998; 21:375–82. [PubMed: 9735945]

Hatten ME. Neuronal inhibition of astroglial cell proliferation is membrane mediated. J Cell Bio. 1985; 100:384–396. [PubMed: 3881455]

Hevner, RF. Reelin and the Cerebellum. In: Fatemi, SH., editor. Reelin Glycoprotein Structure, Biology and Roles in Health and Disease. New York: 2008. p. 141-158.

Hekimi S, Kershaw D. Axonal guidance defects in a *Caenorhabditis elegans* mutant reveal cell-extrinsic determinants of neuronal morphology. J Neurosci. 1993; 13:4254–71. [PubMed: 8410186]

Helms AW, Gowan K, Abney A, Savage T, Johnson JE. Overexpression of MATH1 disrupts the coordination of neural differentiation in cerebellum development. Mol Cell Neurosci. 17:671–682. [PubMed: 11312603]

Higgs HN, Pollard TD. Activation by Cdc42 and PIP_2 of Wiskott-Aldrich syndrome protein (WASp) stimulates actin nucleation by Arp2/3 complex. J Cell Bio. 2000; 150:1311–1320. [PubMed: 10995437]

Innocenti M, Frittoli E, Ponzanelli I, Falck JR, Brachmann SM, Di Fiore PP, Scita G. Phosphoinositide 3-kinase activates Rac by entering in a complex with Eps8, Abi1, and Sos-1. J Cell Bio. 2003; 160:17–23. [PubMed: 12515821]

Innocenti M, Zucconi A, Disanza A, Frittoli E, Areces LB, Steffen A, Stradal TEB, Di Fiore PP, Carlier M, Scita G. Abi1 is essential for the formation and activation of a WAVE2 signalling complex. Nat Cell Bio. 2004; 6:319–327. [PubMed: 15048123]

Ishimura R, Martin GR, Ackerman SL. Loss of apoptosis-inducing factor results in cell-type-specific neurogenesis defects. J Neurosci. 2008; 28:4938–4948. [PubMed: 18463247]

Kaiser ME, Merrill RA, Stein AC, Breburda E, Clagett-Dame M. Vitamin A deficiency in the late gastrula stage rat embryo results in a one to two vertebral anteriorization that extends throughout the axial skeleton. Dev Biol. 2003; 257:14–29. [PubMed: 12710954]

Katsuyama Y, Terashima T. Developmental anatomy of *reeler* mutant mouse. Dev Growth Differ. 2009; 51:271–86. [PubMed: 19379278]

Kawauchi T, Hoshino M. Molecular pathways regulating cytoskeletal organization and morphological changes in migrating neurons. Dev Neurosci. 2008; 30:36–46. [PubMed: 18075253]

Lalonde R, Strazielle C. Brain regions and genes affecting postural control. Prog Neurobiol. 2007; 81:45–60. [PubMed: 17222959]

Luo L. Rho GTPases in neuronal morphogenesis. Nat Rev. 2000; 1:173–180.

Maes T, Barcelo A, Buesa C. Neuron navigator: a human gene family with homology to *unc-53*, a cell guidance gene from *Caenorhabditis elegans*. Genomics. 2002; 80:21–30. [PubMed: 12079279]

McNeill EM, Roos KP, Moechars D, Clagett-Dame M. Nav2 is necessary for cranial nerve development and blood pressure regulation. Neural Dev. 2010; 5:6. [PubMed: 20184720]

Merrill RA, Ahrens JM, Kaiser ME, Federhart KS, Poon VY, Clagett-Dame M. All-*trans* retinoic acid-responsive genes identified in the human SH-SY5Y neuroblastoma cell line and their regulated expression in the nervous system of early embryos. Biol Chem. 2004; 385:605–14. [PubMed: 15318809]

Merrill RA, Plum LA, Kaiser ME, Clagett-Dame M. A mammalian homolog of *unc-53* is regulated by *all-trans* retinoic acid in neuroblastoma cells and embryos. Proc Natl Acad Sci USA. 2002; 99:3422–7. [PubMed: 11904404]

Miale IL, Sidman RL. An autoradiographic analysis of histogenesis in the mouse cerebellum. Exp Neurol. 1961; 4:277–96. [PubMed: 14473282]

Muley PD, McNeill EM, Marzinke MA, Knobel KM, Barr MM, Clagett-Dame M. The atRA-responsive gene neuron navigator 2 functions in neurite outgrowth and axonal elongation. Dev Neurobiol. 2008; 68:1441–53. [PubMed: 18726912]

Nakatsuji N, Nagata I. Paradoxical perpendicular contact guidance displayed by mouse cerebellar granule cell neurons *in vitro*. Development. 1989; 106:441–7. [PubMed: 2689134]

Peeters PJ, Baker A, Goris I, Daneels G, Verhasselt P, Luyten WH, Geysen JJ, Kass SU, Moechars DW. Sensory deficits in mice hypomorphic for a mammalian homologue of unc-53. Brain Res Dev Brain Res. 2004; 150:89–101.

Proepper C, Johannsen S, Liebau S, Dahl J, Vaida B, Bockmann J, Kreutz MR, Gundelfinger ED, Boeckers TM. Abelson interacting protein 1 (Abi-1) is essential for dendrite morphogenesis and synapse formation. EMBO J. 2007; 26:1397–1409. [PubMed: 17304222]

Schmidt KL, Marcus-Gueret N, Adeleye A, Webber J, Baillie D, Stringham EG. The cell migration molecule UNC-53/NAV2 is linked to the ARP2/3 complex by ABI-1. Development. 2009; 136:563–74. [PubMed: 19168673]

See AW, Clagett-Dame M. The temporal requirement for vitamin A in the developing eye: mechanism of action in optic fissure closure and new roles for the vitamin in regulating cell proliferation and adhesion in the embryonic retina. Dev Biol. 2009; 325:94–105. [PubMed: 18955041]

Sillitoe RV, Joyner AL. Morphology, molecular codes, and circuitry produce the three-dimensional complexity of the cerebellum. Annu Rev Cell Dev Biol. 2007; 23:549–77. [PubMed: 17506688]

Stringham E, Pujol N, Vandekerckhove J, Bogaert T. *unc-53* controls longitudinal migration in *C. elegans*. Development. 2002; 129:3367–79. [PubMed: 12091307]

Sudarov A, Joyner A. Cerebellum morphogenesis: the foliation pattern is orchestrated by multi-cellular anchoring centers. Neural Dev. 2007; 2:26. [PubMed: 18053187]

Tahirovic S, Hellal F, Neukirchen D, Hindges R, Garvalov BK, Flynn KC, Stradal TE, Chrostek-Grashoff A, Brakebusch C, Bradke F. Rac1 regulates neuronal polarization through the WAVE complex. J Neurosci. 2010; 30:6930–6943. [PubMed: 20484635]

Takenawa T, Suetsugu S. The WASP-WAVE protein network: connecting the membrane to the cytoskeleton. Nat Rev Mol Cell Bio. 2007; 8:37–48. [PubMed: 17183359]

Trenkner E, Sidman RL. Histogenesis of mouse cerebellum in microwell cultures. Cell reaggregation an dmigration, fiber and synapse formation. J Cell Bio. 1977; 75:915–940. [PubMed: 562889]

van Haren J, Draegestein K, Keijzer N, Abrahams JP, Grosveld F, Peeters PJ, Moechars D, Galjart N. Mammalian Navigators are microtubule plus-end tracking proteins that can reorganize the cytoskeleton to induce neurite-like extensions. Cell Motil Cytoskeleton. 2009; 66:824–38. [PubMed: 19396870]

Wilkinson, D. In situ hybridization: a practical approach. Oxford University Press; New York: 1998.

Witte H, Bradke F. The role of the cytoskeleton during neuronal polarization. Curr Opin Neurobio. 2008; 18:479–487.

Yamasaki T, Kawaji K, Ono K, Bito H, Hirano T, Osumi N, Kengaku M. *Pax6* regulates granule cell polarization during parallel fiber formation in the developing cerebellum. Development. 2001; 128:3133–44. [PubMed: 11688562]

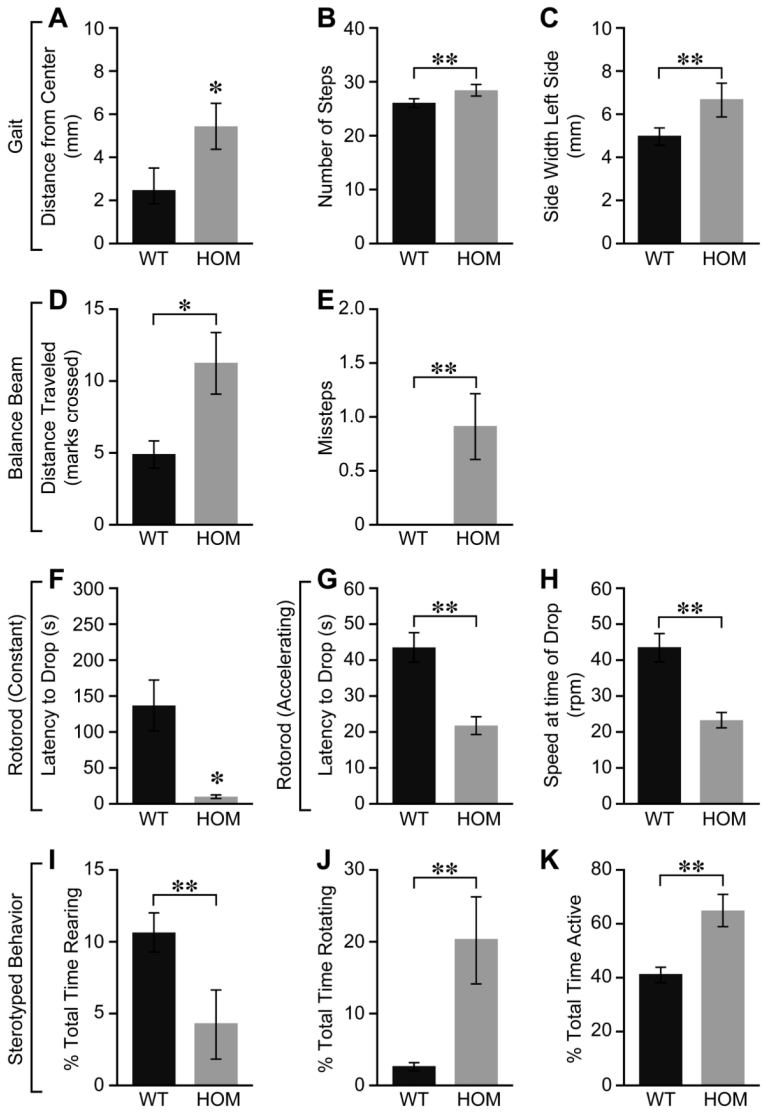

Figure 1.

Nav2$^{-/-}$ hypomorphic mutants exhibit deficits in motor coordination and balance in behavioral tests. (A–C) Gait analysis: mutant mice are off center, take an increased total number of steps and display an increased side width on the left side. (D–E) Mutants display an increased distance traveled on the balance beam and an increased number of missteps relative to wild-type. (F–H) Constant and accelerating rotorod test: mutant mice have a decreased latency to fall and the speed at time of drop is decreased from wild-type animals. (I–K) *Nav2*$^{-/-}$ hypomorphic mutants exhibit deficits in coordination and activity by visual observation in stereotyped behavioral analysis including a decreased percentage of time rearing, and increased percentage of time rotating as well as an increased percentage of time active. * Indicates a p value ≤ 0.05; ** indicates a p value ≤ 0.01; values are mean ± standard error of the mean.

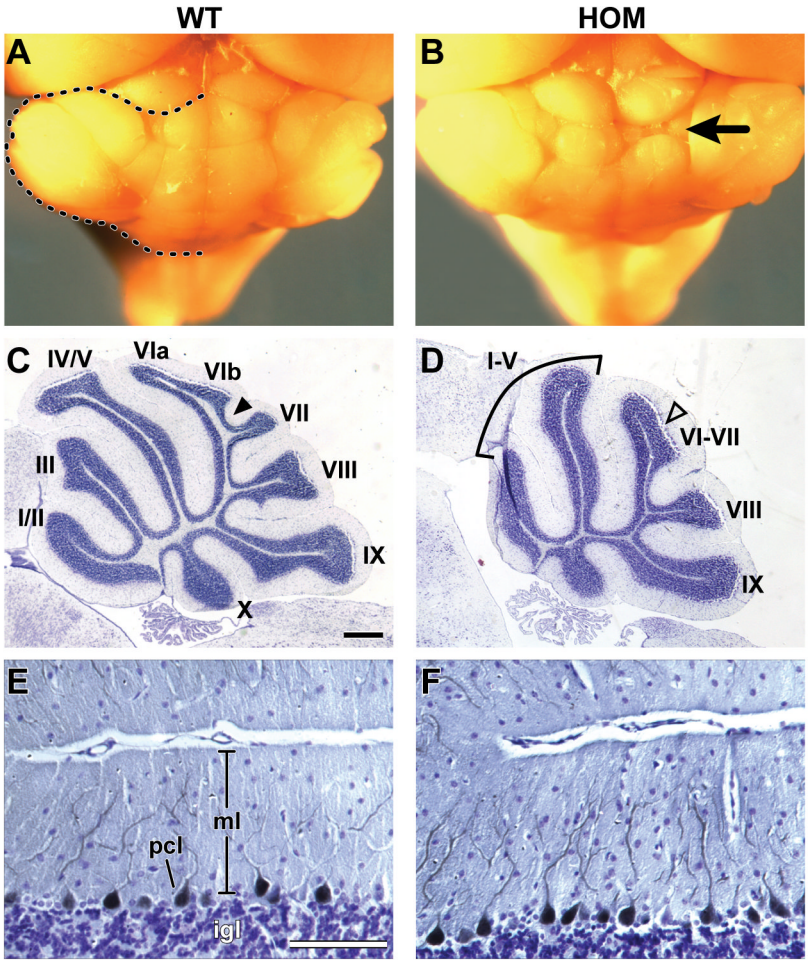

G Foliation Defect

	VI / VII	I - V
WT	0%	0%
HOM	100%	67%

Figure 2.

Cerbellar abnormalities in adult hypomorphic *Nav2*$^{-/-}$ mutants. (A) Wild-type cerebellum (dotted line outlines the left side of the cerebellum). B) Abnormal vermal folding on the right side of an adult *Nav2* mutant cerebellum (black arrow). (C) Normal foliation in the wild-type animal in (A) is shown in a medial cresyl violet-stained sagittal section (10 μm). Note the presence of the intercural fissue (closed arrowhead) separating folia VIb and VII. (D) Abnormal foliation in the mutant shown in (B); note the presence of only 2 folia in the region of I–V in the homozygote compared to 3 distinct folia (I/II, III, and IV/V) in the wild-type; the homozygote also shows a reduction in overall development of VI/VII including the absence of the intercural fissure (open arrowhead, D). (E,F) Overall cytoarchitecture as revealed by cresyl violet staining. The development of the molecular, Purkinje (stained with antibody to calbindin d28k), and granule layers (dark blue). Note the closer spacing of the Purkinje cell bodies in the mutant. (G) The percentage of animals with a defect in foliation in the regions I–V and VI/VII as determined from analysis of medial sagittal sections is shown for wild-type (n = 6) and homozygous mutant (n = 12) mice. igl, inner granule layer;

ml, molecular layer; pcl, Purkinje cell layer. Folia are designated by roman numerals (I/II–X). Scale bars: 100 μm C–F.

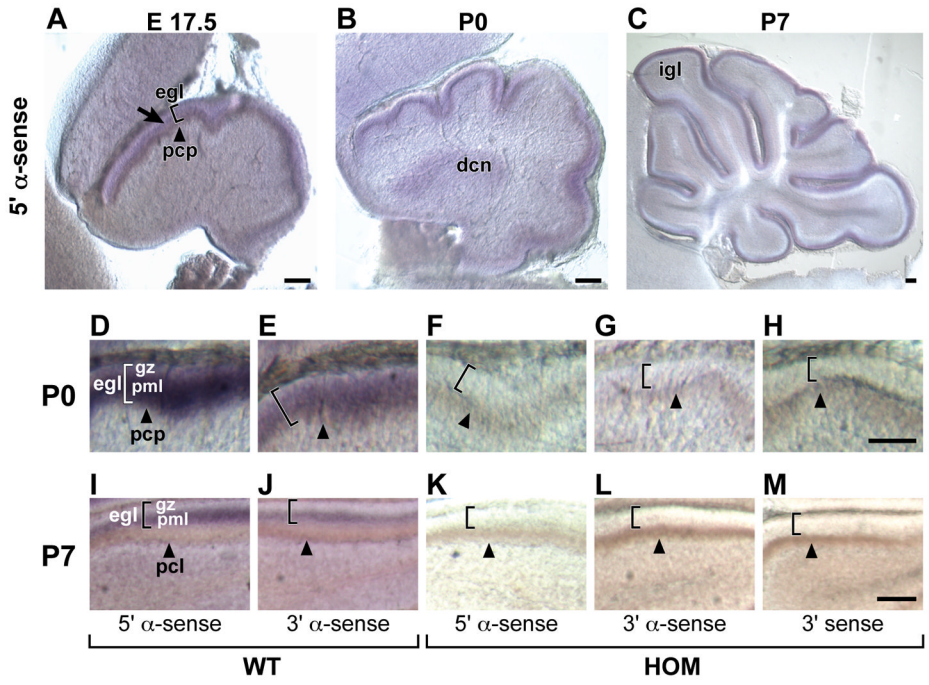

Figure 3.

Nav2 mRNA expression in the embryonic and postnatal cerebellum. (A–C) The *Nav2* transcript in wild-type mice is detected using the 5′ probe in the premigratory granule cells within the EGL (bracket) at E17.5, P0 and P7. Specific staining is also seen in the deep cerebellar nucleus (P0) and the inner granule layer (P7). The location of the Purkinje cell plate (brown) is indicated by the closed arrowhead. Specific *Nav2* staining is shown at P0 and P7 in the inner or pre-migratory cell layer (pml) of the wild-type EGL using both the 5′ (D,I) and 3′ probes (E,J). No specific *Nav2* stain is observed with the 5′ probe in the homozygote at P0 (F) or P7 (K). No *Nav2* staining is detected with the 3′ probe in the homozygote at these times (G,L), nor is any specific staining detected using the 3′ sense control probe (H,M). dcn, deep cerebellar nucleus; igl, inner granule layer, egl, external granule cell layer (bracket); gz, germinal zone; pcl, Purkinje cell layer; pcp, Purkinje cell plate; pml pre-migratory layer. Scale bars: 100 μm.

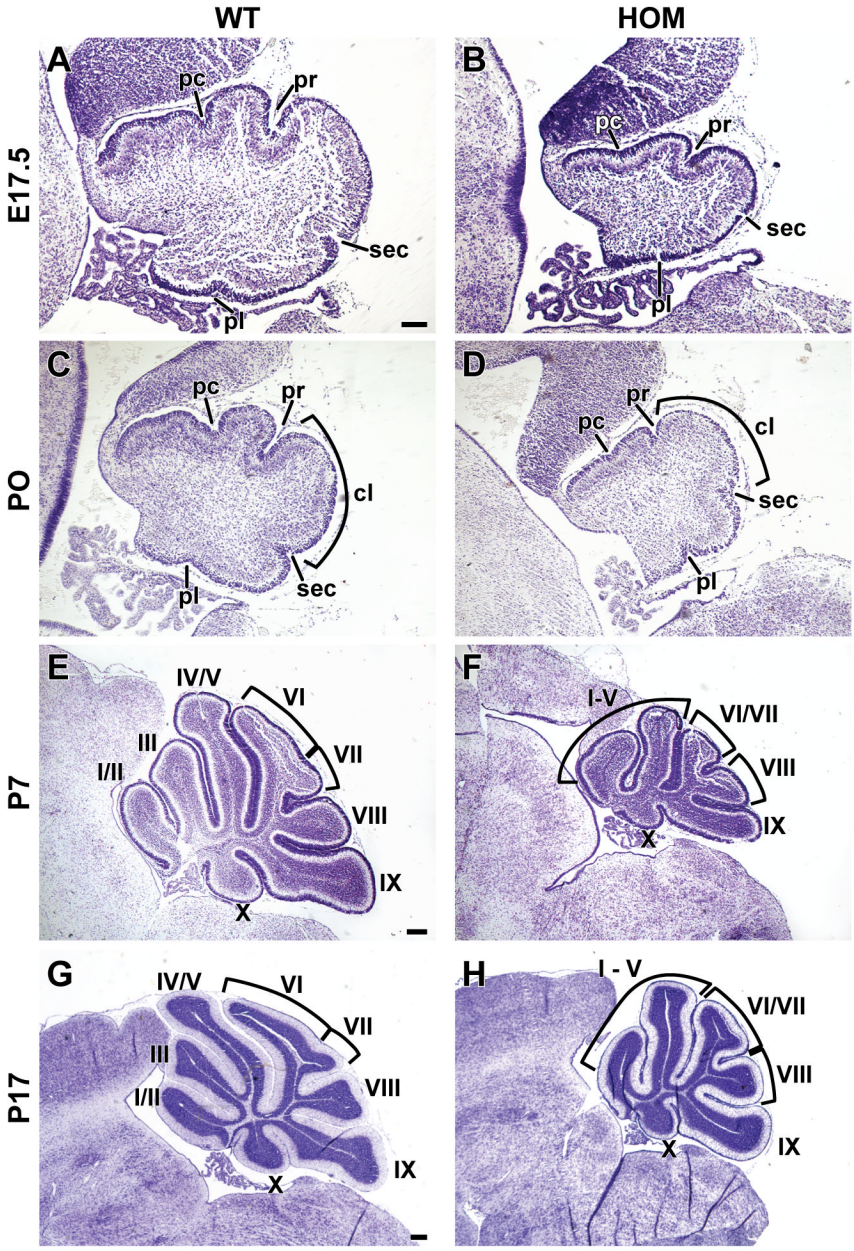

Figure 4.

Morphology of the cerebellum and folia in wild-type and homozygous *Nav2* mice through development. (A–H) Sagittal sections (10 μm) through the medial region of the cerebellum stained with cresyl violet. (A,C) Four fissures are seen in the wild-type cerebellum at E17.5 and P0. (B,D) At E17.5 and P0, the homozygote mutant cerebellum is decreased in size, and fissure formation is delayed; at P0, both the preculminate (pc) and primary (pr) fissures are less well developed compared to the wild-type litter mate control (compare B to A, and D to C). (E–H) At P7 and P17, a lack of tertiary fissure initiation (intercural fissue) delineating folia VI from VII is apparent (compare F to E and H to G). Additionally, formation of secondary fissures delineating I/II, III and IV/V is also lacking in the *Nav2* mutant. The number of wild-type and homozygous embryos/animals examined at E17.5, P0, P7 and P14

is 7,10,3,3 and 9,11,3 and 4, respectively. cl, central lobe; sec, secondary; pl, posterolateral. Scale bars: 100 μm A–D; 200 μm E–H.

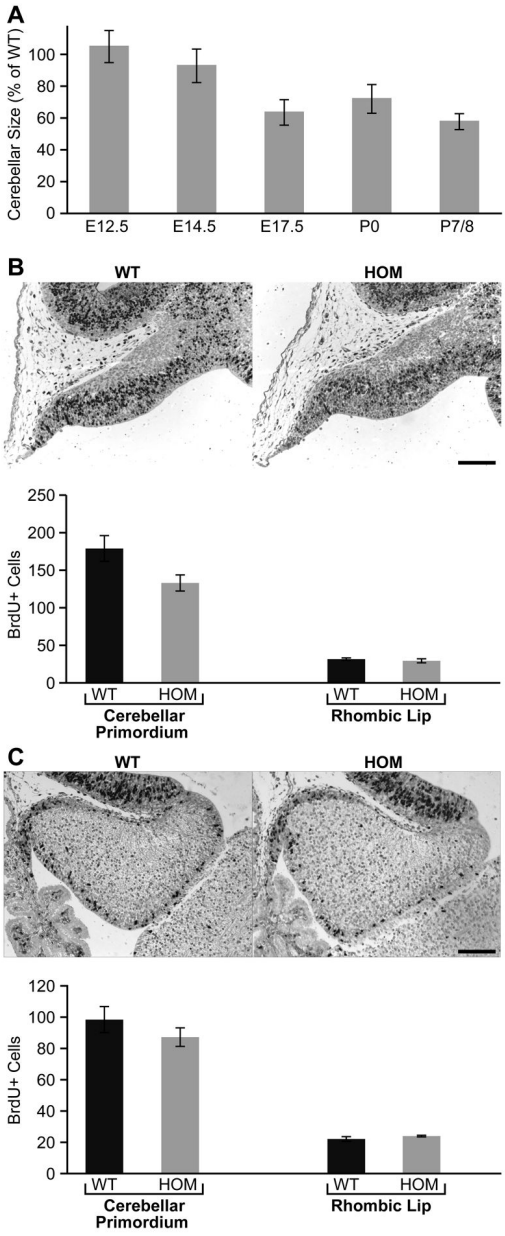

Figure 5.

Development of the cerebellar primordium. (A) Cerebellum size decreases in *Nav2* mutants relative to their wild-type counterparts with advancing development. (B) BrdU positive cells in the cerebellar primordium and rhombic lip at E12.5 in a wild-type and *Nav2* mutant, with the number of labeled cells in each region shown as group averages of wild-type (n=3) and homozygous mutant (n=3) embryos. (C) BrdU positive cells in the cerebellar primordium and rhombic lip at E14.5 in a wild-type and *Nav2* mutant, and quantification of BrdU-labeled cells in each of these areas for wild-type (n=3) and homozygous mutant (n=3) embryos. Scale bars: 100 μm B, C.

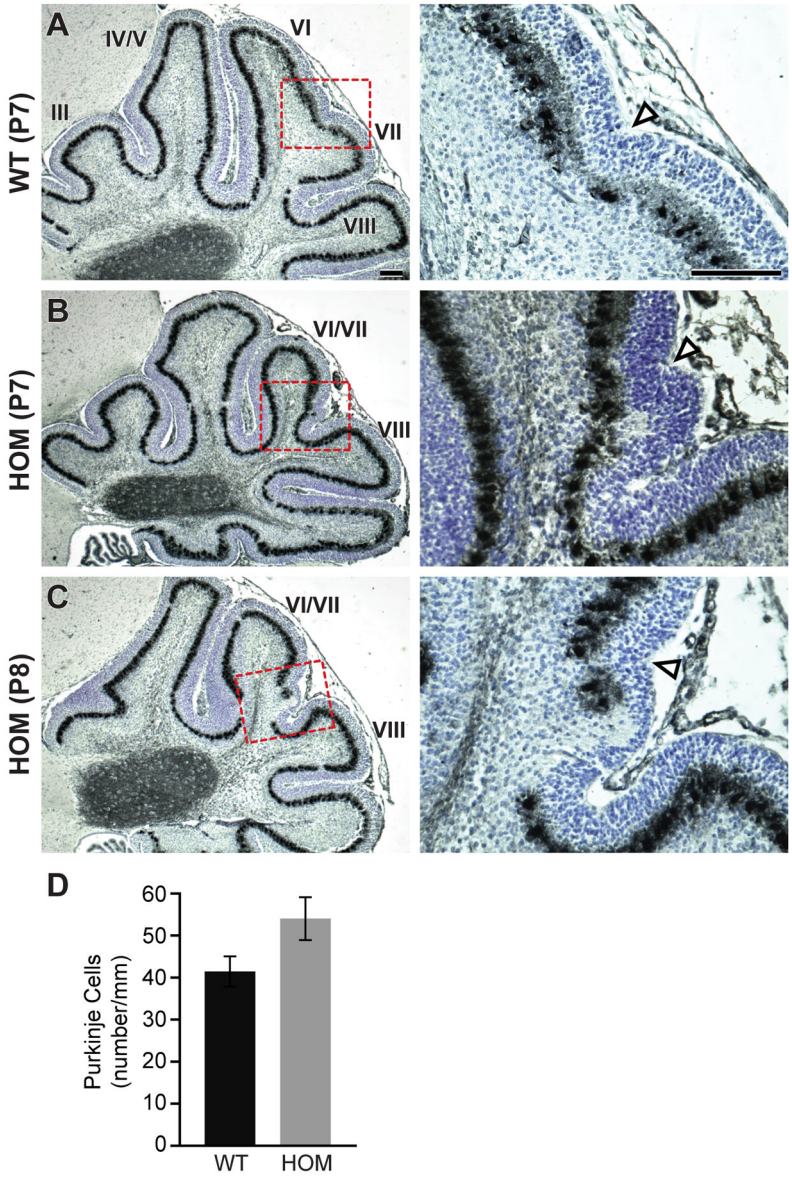

Figure 6.

Purkinje and granule cell abnormalities in *Nav2* mutants at P7 and P8. (A) Calbindin staining of Purkinje cells, and magnification of the region (red box) of the intercural fissure at P7 in a wild-type mouse. (B, C) Calbindin staining at P7 and P8 in *Nav2* hypomorphic mutants; magnification (red box) of abnormal Purkinje cell and granule cell distribution in the region where folia VI should be branching from VII (open white arrow). (D) Total Purkinje cell number as well as tissue circumference was evaluated in sections (3–9/animal) and averaged for each animal (n=3 WT and 4 HOM), and the number of Purkinje cells per mm is shown. Scale bars: 100 μm A–C.

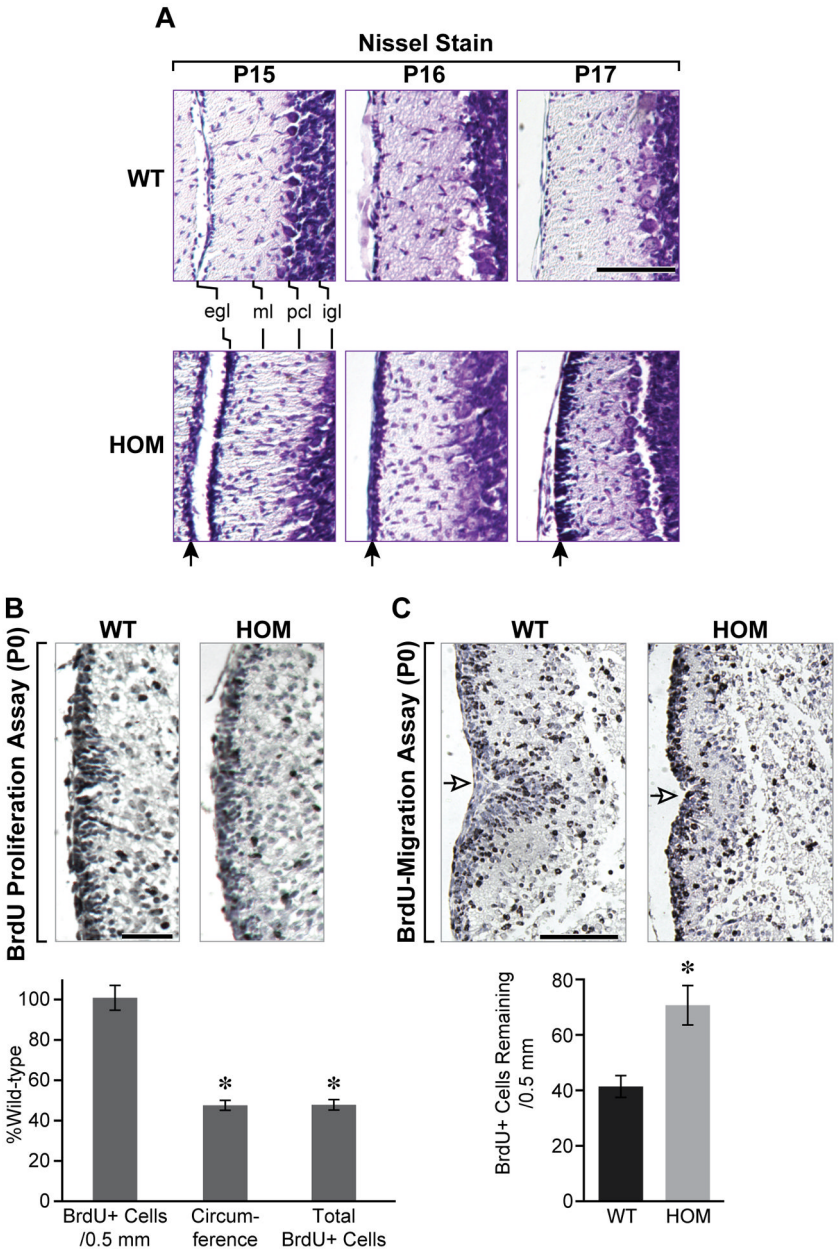

Figure 7.

Migration of the EGL cells is delayed in *Nav2*$^{-/-}$ hypomorphic mutant mice. (A) Cresyl violet-stained sections showing only a small number of cells remaining in the EGL of wild-type controls at P15–16, and absence of the EGL by P17 (n=3, 2 and 3, respectively). In the homozygous mutant, the EGL is thicker than that of the wild-type group at P15–P16 and persists at P17 (black arrow) (n = 2,1 and 3, respectively). (B) Analysis of labeled granule cells 2 h after administration of BrdU to wild-type (n=3) and homozygous mutant (n=3) pups at P0. BrdU positive cells in the proliferating layer (germinal zone) of the EGL in vermal sections were counted, and the circumference of the cerebellum was measured. The graph (bottom left) shows the number of BrdU-stained cells per 0.5 mm of tissue in homozygous mutants (expressed as a percentage of wild-type) does not differ from the wild-type controls; however, the total number of BrdU-labeled cells in the germinal zone of the

entire cerebellum is significantly reduced in *Nav2*$^{-/-}$ mutants. (C) Granule cell migration is defective in *Nav2*$^{-/-}$ mutants. The number of BrdU-labeled granule cells remaining in the proliferating layer of the EGL 40–48 h after maternal injection of BrdU were counted at P0 in wild-type (n=3) and Nav2 mutants (n=3). In the wild-type animal (C, left panel) BrdU-labeled granule cells are dispersed throughout the EGL, and also appear to have moved in the direction of the Purkinje cell plate/IGL. In the *Nav2* hypomorphic mutant littermate (C, right panel), BrdU-labeled cells remain tightly packed in the outer layer of the EGL. The preculminate fissure is indicated by the open arrow. The graph (bottom right) shows the number of BrdU-labeled cells (expressed per 0.5 mm tissue length) remaining in the proliferating layer of the EGL is significantly greater in *Nav2*$^{-/-}$ mutants when compared to wild-type controls. * indicates a p value ≤ 0.02. Scale bars: 50 μm A, B; 100 μm C.

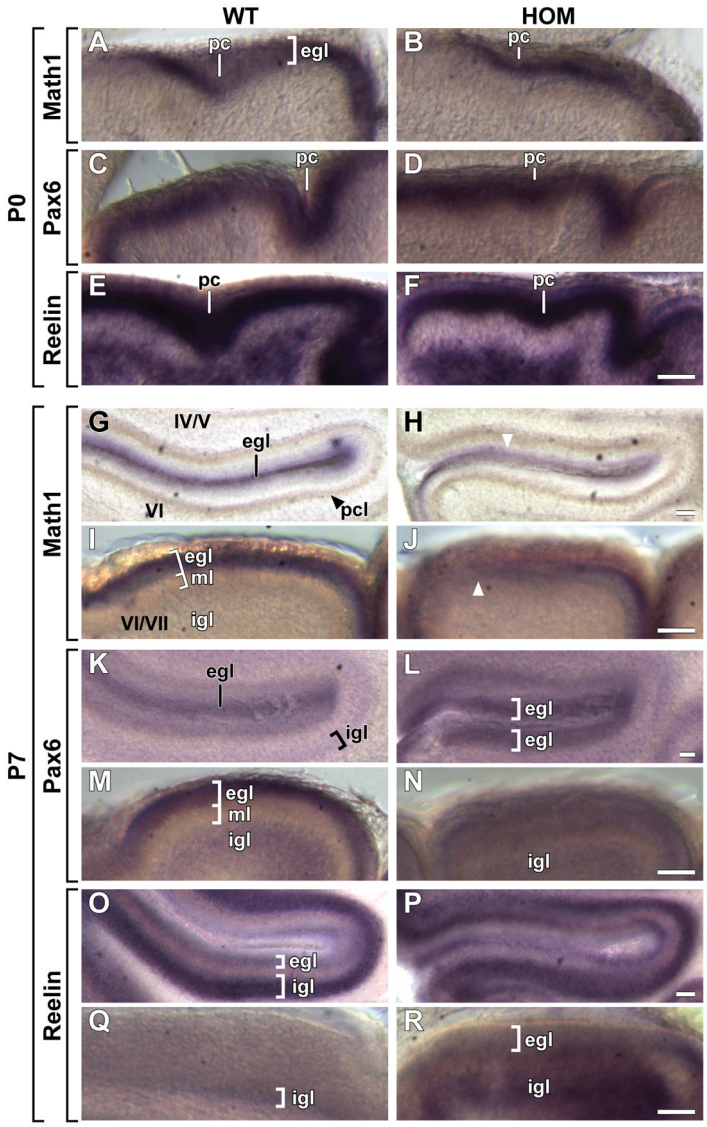

Figure 8.

In situ hybridization of *Math1, Pax6 and Reelin*. (A–F) At P0, wild-type and mutant animals exhibit similar staining in both intensity and distribution (n=3 WT and 2–3 HOM; staining in the region of the preculminate (pc) fissure is shown). (G–R) Transcript expression at P7. (G–J) In the mutant, *Math1* expression is more dispersed (white arrowheads) indicating a lack of organization in both folia IV/V (compare H to G) and VI–VII (compare J to I) in the mutant. (K–R) A failure to form sharp boundaries of Pax6 and Reelin expression in the mutant EGL and IGL is shown in folia IV/V and VI–VII (n= 3 WT and 3 HOM per probe). egl, external granule layer; igl, inner granule layer; ml, molecular layer; pc, preculminate fissure; Scale bars: 50 μm A–R.

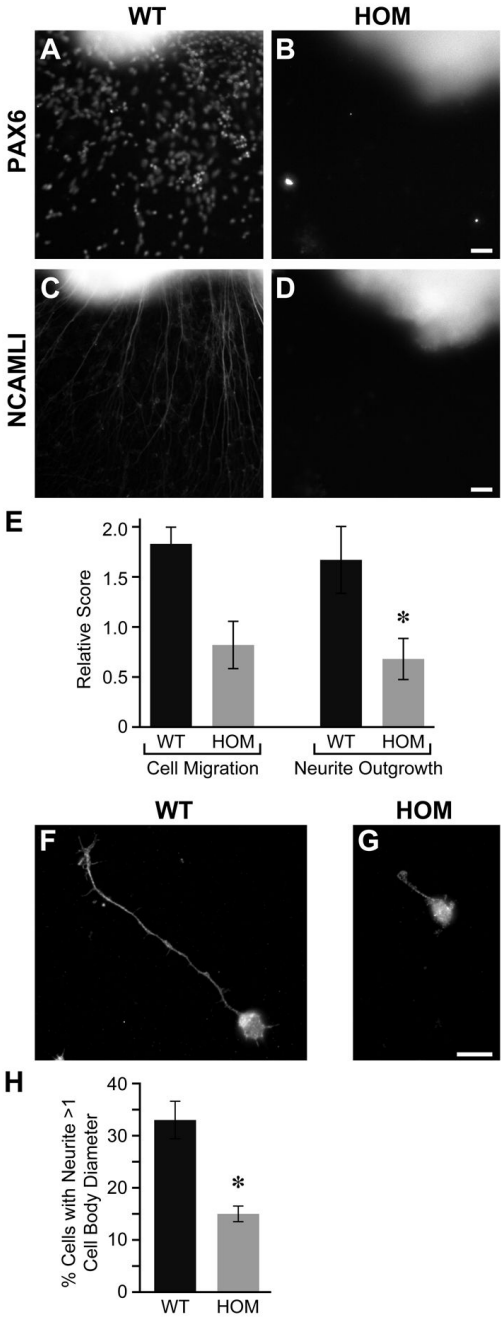

Figure 9.

Granule cell axons are less well developed and granule cells do not migrate normally in *Nav2* mutants. Granule cells stained with an antibody to Pax6 in wild-type (A) and *Nav2* mutant (B) explants after 72 h. Parallel axon fibers stained with NCAM L1 antibody in wild-type (C) and *Nav2* mutant (D) explants after 72 h. Note the absence of neurites and migrating cell bodies in this mutant culture. (E) The migration of cells away from the explant and overall neurite outgrowth was scored in cerebellar explants from 3 wild-type and 11 *Nav2* mutants and there was a significant reduction in neurite outgrowth in homozygous mutant mice. * Indicates a p value ≤ 0.05; Scale bars: 50 μm A–D. (F–G) Dissociated granule cells from wild-type (n = 3) and mutant (n = 3) animals stained with and

antibody to Abi-1. (H) Wild-type mice showed a significantly greater percentage of cells with neurites longer than 1 cell body in diameter. * Indicates a p value ≤ 0.01; Scale bars: 10 μm F–G.